A Quasi-Three-Dimensional Variably Saturated Groundwater Flow Model for Climate Modeling

ZHENGHUI XIE

LASG, Institute of Atmospheric Physics, Chinese Academy of Sciences, Beijing, China

ZHENHUA DI

LASG, Institute of Atmospheric Physics, Chinese Academy of Sciences, and School of Science, Beijing Jiaotong University, Beijing, China

ZHENDONG LUO

Mathematics and Physics Department, North China Electric Power University, Beijing, China

QIAN MA

LASG, Institute of Atmospheric Physics, Chinese Academy of Sciences, Beijing, China

(Manuscript received 31 October 2010, in final form 12 July 2011)

ABSTRACT

In this study, a quasi-three-dimensional, variably saturated groundwater flow model was developed by approximately dividing the three-dimensional soil water and groundwater flow into an unsaturated vertical soil water flow and a horizontal groundwater flow to simulate the interactions among soil water, groundwater, and vegetation. The developed model consists of a one-dimensional unsaturated soil water flow model with the water table as the moving boundary using an adaptive grid structure for a vertical soil column formed based on discrete grid cells in a horizontal domain, a two-dimensional groundwater flow model for the horizontal domain, and an interface model connecting the two components for the horizontal grid cells in the domain. Synthetic experiments by the model were conducted to test the sensitivities of the model parameters of river elevation, ground surface hydraulic conductivity, and surface flux, and the results from the experiments showed the robustness of the proposed model under different conditions. Comparison of the simulation by the model and that by a full three-dimensional scheme showed its feasibility and efficiency. A case of stream water conveyance in the lower reaches of the Tarim River was then applied to validate the developed model for simulation of the water table elevations at the Yingsu section. Finally, a numerical experiment by the model for the Tarim River basin was conducted to discuss the groundwater latent flow for large-scale high-relief topography with stream water conveyance. The results show that the model can simulate the water table reasonably well.

1. Introduction

Dynamic variations in the water table over a region directly influence soil moisture at the surface, which leads to effects on latent and sensible heat fluxes and the growth and development of natural vegetation over the region (Chen and Hu 2004). Water table fluctuations are influenced by surface fluxes such as infiltration or evapotranspiration through the unsaturated zone (e.g., Walko et al. 2000; Sophocleous 2002; York et al. 2002). The role that the water table plays in climate has been implicitly accounted for in several studies (e.g., Salvucci and Entekhabi 1995; Levine and Salvucci 1999; Chen and Kumar 2001; Seuffert et al. 2002; Gedney and Cox 2003; Yang and Niu 2003; Yuan et al. 2008a,b) that have shown the importance of representing shallow groundwater and its interaction with soil moisture in land surface hydrological simulations. Therefore, developing an appropriate groundwater–soil water interaction model

Corresponding author address: Prof./Dr. Zhenghui Xie, LASG, Institute of Atmospheric Physics, Chinese Academy of Sciences, Beijing 100029, China.
E-mail: zxie@lasg.iap.ac.cn

DOI: 10.1175/JHM-D-10-05019.1

for climate modeling will facilitate accurate estimation of water table depths and the improvement of simulations in land surface processes and climate.

The representation of groundwater dynamics in land surface models (LSMs) has received considerable attention in recent years (e.g., Koster et al. 2000; Christiaens and Feyen 2002; Liang and Xie 2003; Ivanov et al. 2004a,b; Maxwell and Miller 2005; Yeh and Eltahir 2005a,b; Rigon et al. 2006; Tian et al. 2006; Fan et al. 2007; Miguez-Macho et al. 2007; Vivoni et al. 2007; Niu et al. 2007; Qu and Duffy 2007; Jones et al. 2008). Liang et al. (2003) established a parameterization to represent unsaturated soil water and groundwater interaction dynamics for the Variable Infiltration Capacity model by reducing it to a moving boundary problem based on the work conducted by Xie et al. (1998). Yang and Xie (2003) reduced the moving boundary problem to a fixed boundary problem via coordinate transformation to reduce its computational cost so that it could be applied to a land surface model for climate studies. The groundwater model developed by Yang and Xie (2003) was also coupled into the regional climate model (RegCM3) to investigate the effects of water table dynamics on regional climate (Yuan et al. 2008a). However, none of these studies provides a dynamic representation of lateral groundwater flow and discharge to streams. A two-dimensional groundwater model with lateral flow was used to construct an equilibrium water table via long-term climatic and geologic forcing (Fan et al. 2007), and groundwater processes with lateral flow were implemented into an existing climate model by linking a groundwater reservoir and a rivers–lakes reservoir with its land surface scheme (Miguez-Macho et al. 2007; Ferguson and Maxwell 2010). Xie and Yuan (2010) proposed a statistical–dynamic scheme to predict the water table elevation in response to stream–aquifer interaction in arid regions. Di et al. (2011) developed a quasi-two-dimensional numerical model based on soil water–groundwater and stream–aquifer interactions to estimate water table depths in profiles subject to stream water conveyance.

In this study, we developed a quasi-three-dimensional, variably saturated groundwater flow model by approximately dividing the three-dimensional soil water and groundwater flow into an unsaturated vertical soil water flow and a horizontal groundwater flow for simulation of the interactions between soil water, groundwater, and vegetation in climate modeling. In the aquifer zone, groundwater flow was simulated with two-dimensional discrete equations, while a one-dimensional Richard's equation was applied to simulate vertical soil water flow for an unsaturated soil column formed based on a horizontal discrete grid cell. These components were connected by the vertical fluxes across the water table in a horizontal grid cell. An adaptive grid refinement method was then developed to keep the water table consistent with the vertical discrete layer interface at all times, which is very important for coupling a land surface model applied for climate modeling with the quasi-three-dimensional, variably saturated groundwater flow model. Physically based distributed models including the fully distributed, triangulated irregular network (TIN)–based Real-time Integrated Basin Simulator (tRIBS) hydrologic model (Ivanov et al. 2004a,b; Vivoni et al. 2007), the terrain-based and distributed hydrological model GEOtop (Rigon et al. 2006), MIKE-SHE (Christiaens and Feyen 2002), the Penn State Integrated Hydrologic Model (PIHM) (Qu and Duffy 2007), and ParFlow (Kollet and Maxwell 2006, 2008; Maxwell et al. 2007) are fully three-dimensional hydrological models. Those models have all been used to diagnose feedbacks and processes in studies driven by particular science questions but are not suitable to be used in current climate models for climate modeling.

This paper is organized as follows: the quasi-three-dimensional variably saturated groundwater flow model considering the soil water–groundwater interactions and groundwater lateral effect is described in section 2. Section 3 discusses the sensitivities of the main parameters of the developed model, its validation, and the groundwater latent flow for large-scale high-relief topography with stream water conveyance for Tarim River basin. The conclusions are given in the last section.

2. A quasi-three-dimensional variably saturated groundwater flow model

In this section, a three-dimensional theoretical model of the interaction between soil water and groundwater is first introduced, after which it is reduced approximately to a quasi-three-dimensional model framework. Finally, numerical algorithms for the quasi-three-dimensional model are presented.

a. The moving boundary problem for the interaction between soil water and groundwater

We assumed that the curved surface Γ at the groundwater table divides the three-dimensional domain Ω into two zones: the unsaturated soil water zone Ω_1 and the underlying saturated groundwater zone Ω_2 (Fig. 1). Therefore, we reduced the soil water and groundwater interaction to a three-dimensional moving boundary problem.

In the unsaturated soil water zone Ω_1, the water balance equation for the soil moisture θ can be written as the following three-dimensional Richard's equations:

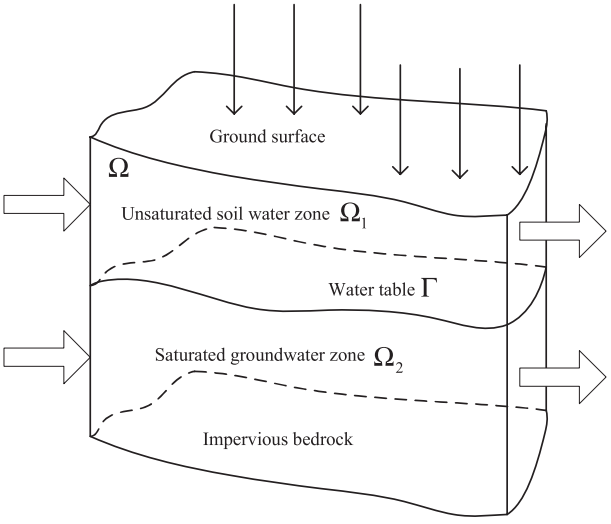

FIG. 1. A schematic diagram of the hydrological system, which includes both the unsaturated soil water zone and the underlying saturated groundwater zone.

$$\frac{\partial\theta}{\partial t} - \nabla\cdot[D(\theta)\nabla\theta] - \frac{\partial K(\theta)}{\partial z} = g(x,y,z), \qquad (1)$$

where $D(\theta)$ is the unsaturated hydraulic diffusivity, $K(\theta)$ is the unsaturated hydraulic conductivity, and $g(x, y, z)$ is the source or sink term.

In the saturated groundwater zone Ω_2, the water balance equation for the water potential ψ can be written as

$$S_s\frac{\partial\psi}{\partial t} - \nabla\cdot(K_s\nabla\psi) - g(x,y,z) = 0, \qquad (2)$$

where S_s is the specific storativity and K_s is the saturated hydraulic conductivity.

For the moving boundary Γ (i.e., the water table Γ), let V_n represent the flow rate in the normal direction at the curved surface for the groundwater table. This can be written as

$$V_n = (q_s - q_u)\cdot\mathbf{n}(t), \qquad (3)$$

where $q_s = -K\nabla\psi$, $q_u = -D(\theta)\nabla\theta$, q_s is the flux in zone Ω_2, q_u is the flux in zone Ω_1, and $\mathbf{n}(t)$ is the unit normal vector on Γ. Equations (1)–(3) with initial and boundary conditions are formulated into the three-dimensional moving boundary problem.

b. A quasi-three-dimensional model framework for the interaction between soil water and groundwater

Based on the three-dimensional theory model described above, we developed a quasi-three-dimensional variably saturated groundwater flow model framework (schematic diagram shown in Fig. 2) to capture the main feature of the soil water flow and groundwater flow quickly that was suitable for climate modeling.

As shown in Fig. 2a, the impervious bedrock Ω' is viewed in the x–y plane (i.e., datum plane), which is divided into grid cells (i.e., a grid cell $\Omega'_1 \subset \Omega'$). If the impervious bedrock is a curved surface, we assume that its projection to the XY plane is Ω'. Because of the effect of gravity in an unsaturated soil water zone, the soil water flow primarily occurs in the vertical direction, and one-dimensional vertical soil columns for the unsaturated soil water zone over the grid cell Ω'_1 are formulated based on the horizontal discrete cells. Groundwater flow in the saturated zone is approximated as horizontal flow over domain Ω'. The vertical flux q links the unsaturated soil water flow and groundwater flow. The model framework was developed by approximately dividing the three-dimensional moving boundary problem into an unsaturated vertical soil water flow problem and a horizontal groundwater flow problem.

1) THE ONE-DIMENSIONAL UNSATURATED SOIL WATER FLOW MODEL FOR A VERTICAL SOIL COLUMN

Let $h(x, y, t)$ and $H(x, y)$ be the water table and the land surface elevation over the grid cell $\Omega'_1 \subset \Omega'$, respectively. A one-dimensional unsaturated water flow for a vertical soil column over the grid cell Ω'_1 can be expressed as follows (e.g., Bear 1972; Lei et al. 1987; Xue et al. 1997):

$$\frac{\partial\theta}{\partial t} = \frac{\partial}{\partial z}\left[D(\theta)\frac{\partial\theta}{\partial z}\right] - \frac{\partial K(\theta)}{\partial z} + f_1(x,y,z,t),$$
$$(x,y)\in\Omega'_1, \quad \text{and} \quad h(x,y,t) < z < H(x,y), \qquad (4)$$

where θ is the soil moisture content, $D(\theta)$ is the unsaturated hydraulic diffusivity, $K(\theta)$ is the unsaturated hydraulic conductivity, $f_1(x, y, z, t)$ is a sink term, and z represents the vertical direction and is assumed to be positive when moving downward.

The initial and boundary conditions for Eq. (4) can be given as follows:

$$\theta(x,y,z,0) = \theta_0(x,y,z), \quad (x,y)\in\Omega'_1,$$
$$z\in(h_0(x,y),H(x,y)), \quad \text{and} \quad t = 0; \qquad (5)$$

$$-D(\theta)\frac{\partial\theta}{\partial z} + K(\theta)|_{z=H(x,y)} = P - E - R, \quad (x,y)\in\Omega'_1,$$
$$z = H(x,y), \quad \text{and} \quad t>0; \quad \text{and} \qquad (6)$$

$$\theta|_{z=h(x,y,t)} = \theta_s, \quad (x,y)\in\Omega'_1, \quad z = h(x,y,t), \quad \text{and} \quad t>0, \qquad (7)$$

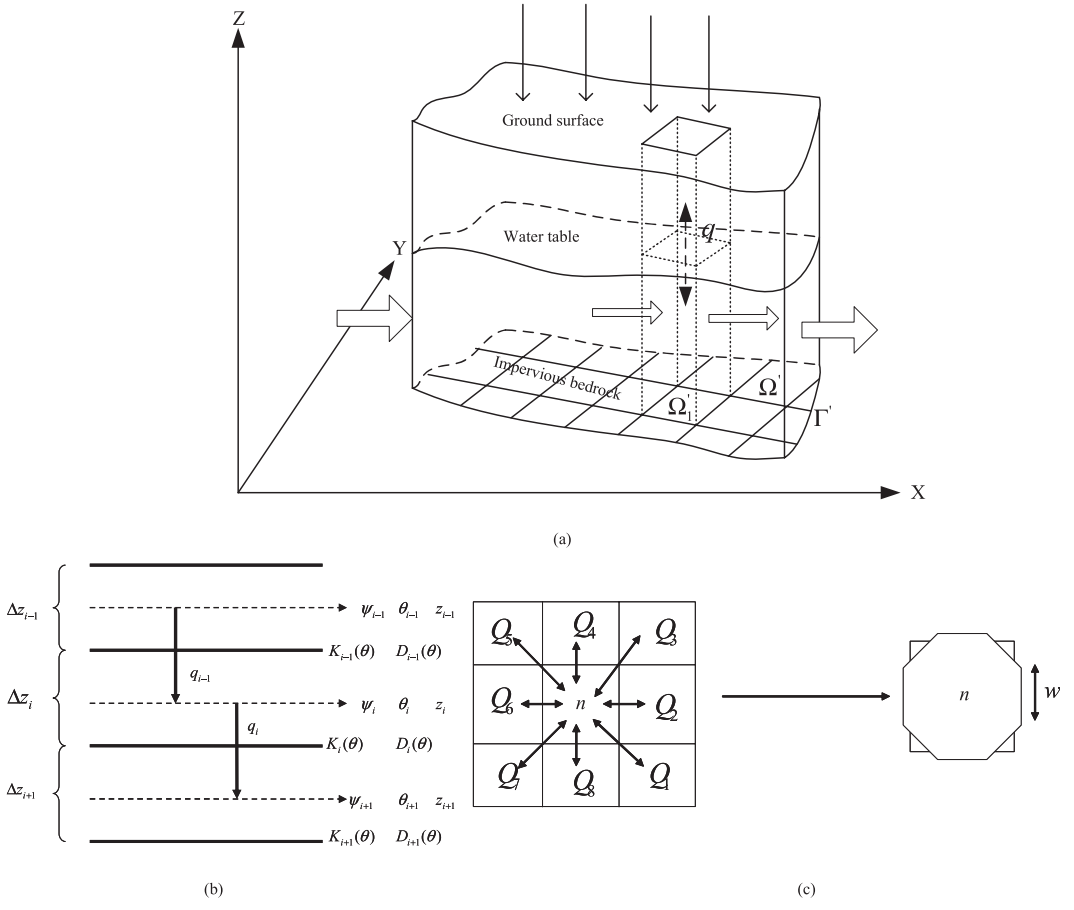

FIG. 2. (a) A quasi-three-dimensional numerical model framework with the interaction between soil water and groundwater, (b) schematic diagram of the numerical scheme used to solve for the soil moisture content in CLM3, and (c) plan views of the lateral groundwater flow for the nth cell and the regular octagon replacing the regular square grid cell.

where $\theta_0(x, y, z)$ and $h_0(x, y)$ are the initial soil moisture and water table elevation in the vertical soil column, θ_s is saturated soil moisture content, P is the rainfall reaching the soil surface, E is the ground evaporation, and R is the surface runoff.

2) THE TWO-DIMENSIONAL GROUNDWATER FLOW MODEL

For the saturated groundwater flow over the horizontal domain Ω', integrating saturated water Eq. (2) from the impervious bedrock to the water table $h(x, y, t)$ based on the Dupuit approximation (Shen et al. 1982) gives

$$n_e\frac{\partial h}{\partial t} = \frac{\partial}{\partial x}\left(K_s h\frac{\partial h}{\partial x}\right) + \frac{\partial}{\partial y}\left(K_s h\frac{\partial h}{\partial y}\right) - q_{z=h(x,y,t)}(x, y, z, t) + f_2(x, y, t) \quad \text{and} \quad (x, y) \in \Omega', \tag{8}$$

where n_e is the specific yield, $h(x, y, t)$ is the water table elevation and mean water potential in z direction, K_s is the saturated hydraulic conductivity, $f_2(x, y, t)$ is a sink term, and $q_{z=h(x,y,z)}(x, y, z, t)$ is the exchange flux between the unsaturated zone and saturated zone across the water table Γ.

The initial and boundary conditions for Eq. (8) can be written in a general formulation as follows:

$$h(x, y, 0) = h_0(x, y), \quad (x, y) \in \Omega', \quad \text{and} \quad t = 0; \quad \text{and} \tag{9}$$

$$-(K_s h_{\Gamma'}\nabla h_{\Gamma'})\cdot\mathbf{n} + \alpha h_{\Gamma'} = Q_{\Gamma'}, \quad (x, y) \in \Gamma', \quad \text{and} \quad t > 0, \tag{10}$$

where $h_0(x, y)$ is the initial water table elevation; Ω' and Γ' represent the inner domain and boundary of the datum plane, respectively; $h_{\Gamma'}$ is the water table elevation on the boundary Γ'; K_s is the saturated hydraulic conductivity; $\mathbf{n}$ is a unit normal vector of the boundary Γ'; α is a parameter that defines the type of boundary condition; and $Q_{\Gamma'}$ is the prescribed flux values at boundary Γ'.

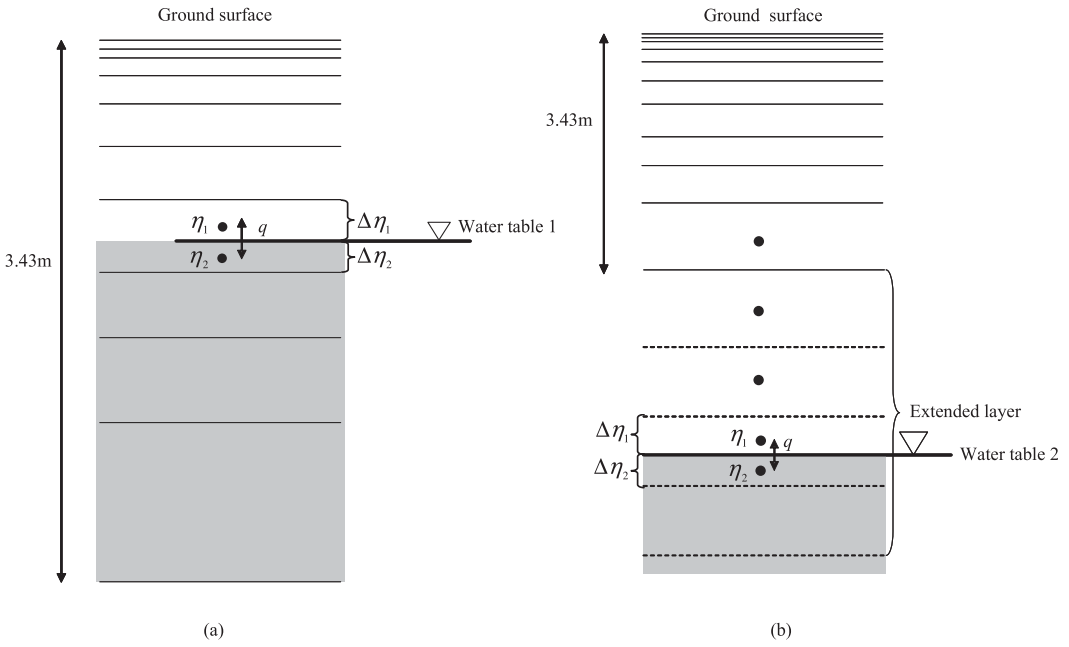

FIG. 3. (a) Soil water flux across the water table in the 10-layer soil column and (b) the extended soil column and soil water flux across the water table.

3) THE CONNECTION EQUATION

In each grid cell, the vertical flux across the water table can be obtained by integrating Eq. (4) over the unsaturated soil column elevation $[h(x, y, t), H(x, y)]$:

$$q_{z=h(x,y,t)}(x,y,z,t) = \int_{h(x,y,t)}^{H(x,y)} \frac{\partial\theta}{\partial t}\, dz + q_{z=H(x,y)}(x,y,z,t). \tag{11}$$

Equation (11) connects the soil water flow problem [Eqs. (4)–(7)] with the groundwater flow problem [Eqs. (8)–(10)].

c. Numerical algorithms for the quasi-three-dimensional model

1) AN ADAPTIVE GRID STRUCTURE FOR THE UNSATURATED SOIL WATER FLOW MODEL WITH WATER TABLE AS THE MOVING BOUNDARY

For each unsaturated soil column $(x, y) \in$ a grid cell $\Omega_1' \subset \Omega'$, the column is divided into m layers from the ground surface, and each layer thickness is $\Delta z_1, \Delta z_2, \ldots, \Delta z_m$. In this study, we extended the 10 soil layers of the Community Land Model, version 3 (CLM3) land surface model (Oleson et al. 2004) to the groundwater zone using the water table as the bottom boundary condition with an adaptive grid refinement method to develop an adaptive grid structure for the unsaturated soil water flow model for the grid cell Ω_1' with the water table as the moving boundary.

The soil column with a depth of 3.43 m was divided into 10 layers, and the node depths z_j(m) ($j = 1, 2, \ldots, 10$) in the jth layer are defined as

$$z_j = 0.025 \times \{\exp[0.5(j - 0.5)] - 1\} \quad \text{and} \quad j = 1, 2, \ldots, 10. \tag{12}$$

The thickness of each layer Δz_j (m) ($j = 1, 2, \ldots, 10$) was defined as follows:

$$\Delta z_j = \begin{cases} 0.5(z_1 + z_2), & j = 1; \\ 0.5(z_{j+1} - z_{j-1}), & j = 2, 3, \ldots 9; \\ z_{10} - z_9, & j = 10. \end{cases} \tag{13}$$

The depths of the layer interfaces $z_{h,j}$ (m) were

$$z_{h,j} = \begin{cases} 0.5(z_j + z_{j+1}), & j = 1, 2, \ldots 9; \\ z_{10} + 0.5\Delta z_{10}, & j = 10. \end{cases} \tag{14}$$

The three soil layers $j - 1$, j, and $j + 1$ are shown in Fig. 2b. Soil moisture is defined at the layer node depth z_j ($j = 1, 2, \ldots, 10$). The hydraulic diffusivity $D(\theta)$, the hydraulic conductivity $K(\theta)$, and the soil water flux q, which is assumed to be positive downward, are defined at the interface depth $z_{h,j}$ ($j = 1, 2, \ldots, 10$).

Using the water table as the bottom boundary of the unsaturated flow problem, we extended the 10 soil layers mentioned above to the groundwater zone in two cases according to the water table positions using an adaptive grid

refinement method. In the first case, the water table is in the 10-layer soil column (Fig. 3a), while in the second case, the water table is below the 10-layer soil column (Fig. 3b).

As shown in Fig. 3a, the water table in the 10-layer soil column is defined as ''water table 1.'' The layer including water table 1 is divided into two new layers: an unsaturated upper portion and a lower saturated portion. The thicknesses of these layers are defined as $\Delta\eta_1$ and $\Delta\eta_2$, respectively. The new nodes (i.e., η_1 and η_2) are located at the middle position of the two new layers, respectively. Obviously, the soil water content in the lower saturated potion is saturated. Thus, Eq. (4) is numerically solved for soil water content as the new soil layer structure, and the saturated soil water content at node η_2 remains constant as the lower boundary condition of Eq. (4). Finally, the two new layers are combined into one layer, which is one of the original 10 soil layers, and the soil water content at the combined layer node is written as

$$\theta = (\theta_{\eta_1}\Delta\eta_1 + \theta_s\Delta\eta_2)/\Delta z, \tag{15}$$

where θ_{η_1} is the soil water content at node η_1, and θ_s is the saturated soil water content at node η_2.

For the water table below the 10-layer soil column, which is designated ''water table 2'' in Fig. 3b, we added an extended layer that includes the soil column from 3.43 m to water table 2 and then divided it into several layers with the same thickness as the tenth layer. Water table 2 is in one of those layers, and separates the layer into two new layers. The soil water content above water table 2 is numerically solved as for the case of water table 1.

2) THE QUASI-THREE-DIMENSIONAL MODEL NUMERICAL ALGORITHMS

We used the regular square division in this study. For one unsaturated soil column over the regular square cell $\Omega_1' \subset \Omega'$, we assumed that the column was divided into m layers from the ground surface to the water table as in the previous discussion and $f_1(x, y, z, t)$ is equal to zero. Therefore, the unsaturated soil water discretion equations could be written as follows:

$$\frac{\theta_j^{k+1} - \theta_j^k}{\Delta t} = \frac{D_{j+1/2}^{k+1}\left(\dfrac{\theta_{j+1}^{k+1} - \theta_j^{k+1}}{z_{j+1} - z_j}\right) - K_{j+1/2}^{k+1} + q_{j-1/2}^{k+1}}{\Delta z_j} \quad \text{and} \quad j = 1, \tag{16}$$

$$\frac{\theta_j^{k+1} - \theta_j^k}{\Delta t} = \frac{D_{j+1/2}^{k+1}\left(\dfrac{\theta_{j+1}^{k+1} - \theta_j^{k+1}}{z_{j+1} - z_j}\right) - D_{j-1/2}^{k+1}\left(\dfrac{\theta_j^{k+1} - \theta_{j-1}^{k+1}}{z_j - z_{j-1}}\right)}{\Delta z_j} - \frac{K_{j+1/2}^{k+1} - K_{j-1/2}^{k+1}}{\Delta z_j} \quad \text{and} \quad j = 2, 3, \ldots, m-1, \quad \text{and} \tag{17}$$

$$\frac{\theta_j^{k+1} - \theta_j^k}{\Delta t} = \frac{D_{j+1/2}^{k+1}\left(\dfrac{\theta_s - \theta_j^{k+1}}{z_{j+1} - z_j}\right) - D_{j-1/2}^{k+1}\left(\dfrac{\theta_j^{k+1} - \theta_{j-1}^{k+1}}{z_j - z_{j-1}}\right)}{\Delta z_j} - \frac{K_{j+1/2}^{k+1} - K_{j-1/2}^{k+1}}{\Delta z_j} \quad \text{and} \quad j = m. \tag{18}$$

Let

$$a_1 = 0, \quad b_1 = 1 + \frac{\Delta t D_{3/2}^{k+1}}{\Delta z_1(z_2 - z_1)}, \quad c_1 = -\frac{\Delta t D_{3/2}^{k+1}}{\Delta z_1(z_2 - z_1)}, \quad \text{and} \quad \delta_1 = \theta_1^k - \frac{\Delta t}{\Delta z_1}(K_{3/2}^{k+1} - q_{1/2}^{k+1});$$

$$a_j = -\frac{\Delta t D_{j-1/2}^{k+1}}{\Delta z_j(z_j - z_{j-1})}, \quad b_j = 1 + \frac{\Delta t D_{j+1/2}^{k+1}}{\Delta z_j(z_{j+1} - z_j)} + \frac{\Delta t D_{j-1/2}^{k+1}}{\Delta z_j(z_j - z_{j-1})}, \quad c_j = -\frac{\Delta t D_{j+1/2}^{k+1}}{\Delta z_j(z_{j+1} - z_j)},$$

$$\delta_j = \theta_j^k - \frac{\Delta t}{\Delta z_j}(K_{j+1/2}^{k+1} - K_{j-1/2}^{k+1}), \quad \text{and} \quad j = 2, 3, \ldots, m-1; \quad \text{and}$$

$$a_m = -\frac{\Delta t D_{m-1/2}^{k+1}}{\Delta z_m(z_m - z_{m-1})}, \quad b_m = 1 + \frac{\Delta t D_{m+1/2}^{k+1}}{\Delta z_m(z_{m+1} - z_m)} + \frac{\Delta t D_{m-1/2}^{k+1}}{\Delta z_m(z_m - z_{m-1})}, \quad \text{and}$$

$$\delta_m = \theta_m^k + \frac{\Delta t D_{m+1/2}^{k+1}\theta_s}{\Delta z_m(z_{m+1} - z_m)} - \frac{\Delta t}{\Delta z_m}(K_{m+1/2}^{k+1} - K_{m-1/2}^{k+1}).$$

Thus, Eqs. (16)–(18) are expressed as follows:

$$\begin{cases} b_1\theta_1^{k+1} + c_1\theta_2^{k+1} = \delta_1, \\ a_j\theta_{j-1}^{k+1} + b_j\theta_j^{k+1} + c_j\theta_{j+1}^{k+1} = \delta_j, \quad j = 2,3, \ldots, m-1, \\ a_m\theta_{m-1}^{k+1} + b_m\theta_m^{k+1} = \delta_m. \end{cases} \tag{19}$$

The discrete equations for other soil columns were formulated in a similar way.

For a regular square cell $\Omega_1' \subset \Omega'$, each cell has eight neighbor cells. To simulate the groundwater lateral flow reasonably, we assumed that the chance of lateral flow among grid cells was equal, and the regular square cell was replaced by the regular octagon S with the same area of the grid cell to calculate the width (w) of the flow cross section between two cells (see Fig. 2c). The width w is calculated by $w = \Delta x\sqrt{0.5\tan(\pi/8)}$, where Δx is the side length of the regular square cell. For the two-dimensional groundwater flow, integrating Eq. (8) over the horizontal discrete grid S on the datum plane and using the regular octagon S gives

$$\iint_S n_e\frac{\partial h}{\partial t}\,dS = \int_{\partial S}\left(K_s h\frac{\partial h}{\partial x}, K_s h\frac{\partial h}{\partial y}\right)\cdot \mathbf{n}\,dS - \iint_S [q_{z=h(x,y,t)}(x,y,z,t) - f_2(x,y,t)]\,dS, \tag{20}$$

where $\mathbf{n}$ is the normal vector for eight sides of the regular octagon S. The area of S is that of a regular square grid cell with length Δx and width Δy (i.e., $\Delta x = \Delta y$).

Averaging the equation with the cell area and representing the direction derivatives by the water tables at the neighbor cells gives

$$n_e\frac{dh}{dt} = \frac{1}{\Delta x\Delta y}\sum_{i=1}^{8} wK_s h(i)\left[\frac{h(i) - h}{l}\right] - q_{z=h(x,y,t)}(x,y,z,t) + f_2(x,y,t), \tag{21}$$

where $h(i)$ is the water table elevation in the ith cell counted counterclockwise around the center cell (i.e., the S cell), l is the distance between two cell nodes—that is, $l = \Delta x$ along x or y, and $l = \sqrt{2}\Delta x$ along the diagonal—and the flow transmissivity $T(i) = K_s h(i)$. To ensure that flow from cell S to the ith cell is the same as from the ith cell to S under the same hydraulic conductivity, $T(i)$ is calculated for both cells involved and the average of the two is used.

An implicit difference scheme of Eq. (21) for the entire horizontal plane can be written as

$$n_e\frac{h_n^{k+1} - h_n^k}{\Delta t} = \frac{1}{\Delta x\Delta y}\sum_{i=1}^{8} wT_n^{k+1}(i)\left[\frac{h_n^{k+1}(i) - h_n^k}{l}\right] - q_{z=h(n,t)}^{k+1}(n) + f_n^{k+1}; \quad n = 1,2,\ldots,N; \quad \text{and} \quad k = 1,2,\ldots, \tag{22}$$

where N is the total number of horizontal discrete cells, k is time step number, $T_n(i)$ is the average flow transmissivity between the nth cell and its ith cell counterclockwise, and f_n^{k+1} is a sink term in the nth cell.

In each horizontally discrete cell, the discretization of connection Eq. (11) can be expressed as follows:

$$q_{z=h(n,t)}^{k+1}(n) = \sum_{j=1}^{m}\frac{\theta_j^{k+1}(n) - \theta_j^k(n)}{\Delta t}\Delta z_j + q_{z=H(n)}^{k+1}(n); \quad n = 1,2,\ldots,N; \quad \text{and} \quad k = 1,2,\ldots, \tag{23}$$

where $q_{z=H(n)}^{k+1}(n)$ is the ground surface flux in the nth cell at time $(k+1)\Delta t$ (i.e., a uniform time step is adopted).

We now describe how to dynamically compute the soil moisture content θ and water table elevation h at the next time $t + \Delta t$ with known θ and h at time t. The numerical procedures can be briefly summarized as follows:

(i) Assume that the values of the soil moisture content $\theta(n,j,t)$ ($j = 1,2,\ldots,m$; $n = 1,2,\ldots,N$) and water table elevation $h(n,t)$ ($n = 1,2,\ldots,N$) at time t are given. Fix $h(n,t)$ in a horizontal grid cell, I_n($n = 1, 2, \ldots, N$), and then compute the preestimate value $\theta'(n,j,t+\Delta t)$ ($j = 1,2,\ldots,m$) with Eq. (19) from $\theta(n,j,t)$ and $h(n,t)$. Iterate on $\theta'(n,j,t+\Delta t)$ ($j = 1, 2, \ldots, m$) until it converges.

(ii) Compute the preestimate value $q'_{z=h(n,t)}(n,t+\Delta t)$ of flux across the water table in the horizontal grid cell I_n with Eq. (23) from $\theta(n,j,t)$, and $\theta'(n,j,t+\Delta t)$ ($j = 1, 2, \ldots, m$) in step (i), and provide the surface flux.

(iii) Repeat steps (i) and (ii) in each horizontal grid cell I_n ($n = 1,2,\ldots,N$), then put all of $q'_{z=h(n,t)}(n,t+\Delta t)$ ($n = 1, 2, \ldots, N$) into Eq. (22) to compute the preestimate value $h'(n,t+\Delta t)$ ($n = 1, 2, \ldots, N$) with $h(n,t)$ ($n = 1, 2, \ldots, N$) as iterative initial values. Next, update the iterative preestimate value of the soil moisture content $\theta'(n,j,t+\Delta t)$ ($j = 1, 2, \ldots, m$) corresponding to the elevation and decline of the water table.

(iv) Take $\theta'(n,j,t+\Delta t)$ ($j = 1, 2, \ldots, m$) and $h'(n,t+\Delta t)$ ($n = 1, 2, \ldots, N$) as the iterative values of Eqs. (19) and (22), and repeat steps (i)–(iii) until $\theta'(n,j,t+\Delta t)$ ($j = 1,2,\ldots,m$) and $h'(n,t+\Delta t)$

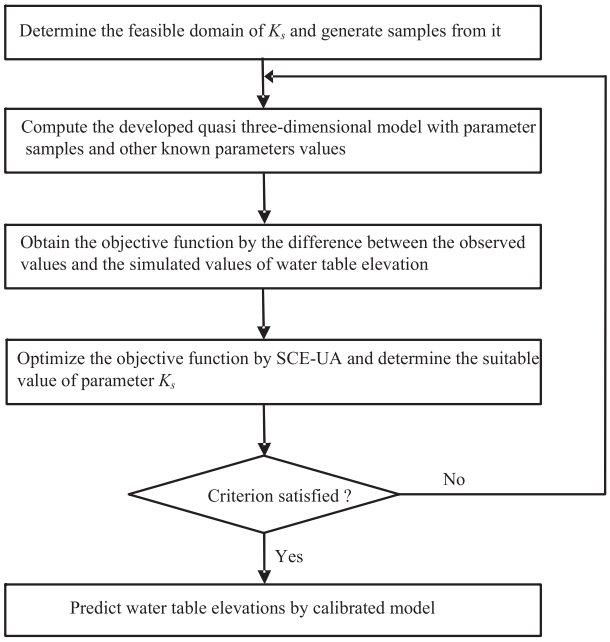

FIG. 4. Flowchart for the water table elevation prediction based on the developed model and SCE-UA.

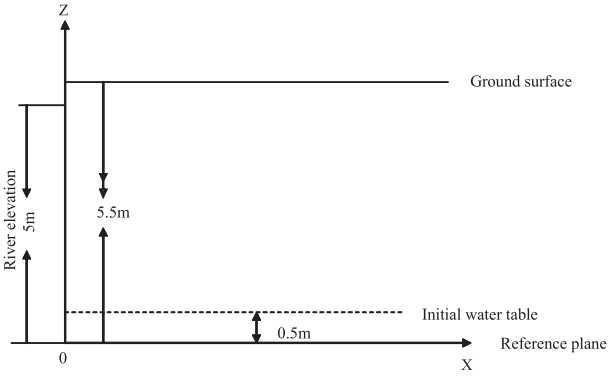

FIG. 5. The cross-sectional profile of the aquifer zone.

$(n = 1, 2, \ldots, N)$ converge. Then $\theta'(n, j, t + \Delta t)$ $(j = 1, 2, \ldots, m; n = 1, 2, \ldots, N)$ and $h'(n, t + \Delta t)$ $(n = 1, 2, \ldots, N)$ are the correct values of soil moisture content and water table elevations at time $t + \Delta t$, respectively.

(v) Repeat steps (i)–(iv) for the next time step.

3) AN ESTIMATION SCHEME OF WATER TABLE DEPTH BASED ON THE DEVELOPED MODEL AND SCE-UA METHOD

Based on the quasi-three-dimensional numerical model, we present an estimation scheme of water table depth that first applies the shuffled complex evolution method developed at the University of Arizona (SCE-UA) (e.g., Duan et al. 1992, 1994) to calibrate the main parameters of the model, such as the groundwater hydraulic conductivity K_s, which is then used to predict water table elevations by model. The scheme flowchart is shown in Fig. 4. The water table elevation obtained by the model can be easily converted into water table depth based on the difference between the surface soil elevation and water table elevation.

3. Model validations

a. Sensitivities of model parameters

Sensitivity analyses of the model parameters were conducted prior to testing the developed soil water–groundwater interaction model. The study domain was a rectangular parallelepiped aquifer zone 50 m from the river bank that was 10 m wide and 5.5 m deep from the ground surface nearest the river bank. We assumed that impervious bedrock was the reference plane. The vertical space step was assigned as described in section 2c, the uniform horizontal space step Δx (or Δy) is 1 m, and the uniform time step Δt is 0.5 h. The river is 5 m deep to the reference plane, and the initial water table depth is 5 m (Fig. 5). The sink terms $f_1(x, y, z, t)$ and $f_2(x, y, t)$ are zero.

We computed the flow transmissivity T in the nth cell as follows (Fan et al. 2007):

$$T_n = \int_{d_n}^{\infty} K_s \, dz = \int_{d_n}^{\infty} K_0 \exp(-z/f) \, dz = K_0 f e^{-d_n/f}, \tag{24}$$

where d_n is the water table depth, and K_s is the groundwater hydraulic conductivity in the horizontal direction, which is parameterized as

$$K_s = K_0 \exp(-z/f), \tag{25}$$

where K_0 is the groundwater hydraulic conductivity for the surface soil, z is the depth from the surface, and f is the e-folding length. The magnitude of f depends on many factors, which can be given as follows (refer to Fan et al. 2007):

$$f = \begin{cases} \dfrac{120}{1 + 150\beta} \text{ m}, & \text{for} \quad \beta \le 0.16; \\ 5 \text{ m}, & \text{for} \quad \beta > 0.16. \end{cases} \tag{26}$$

In the unsaturated soil column, the hydraulic diffusivity $D(\theta)$ and the hydraulic conductivity $K(\theta)$ are parameterized based on the empirical relationships (Clapp and Hornberger 1978) as $D(\theta) = -(bK_{s1}\psi_s/\theta_s)(\theta/\theta_s)^{b+2}$ and $K(\theta) = K_{s1}(\theta/\theta_s)^{2b+3}$, where K_{s1} is the saturated

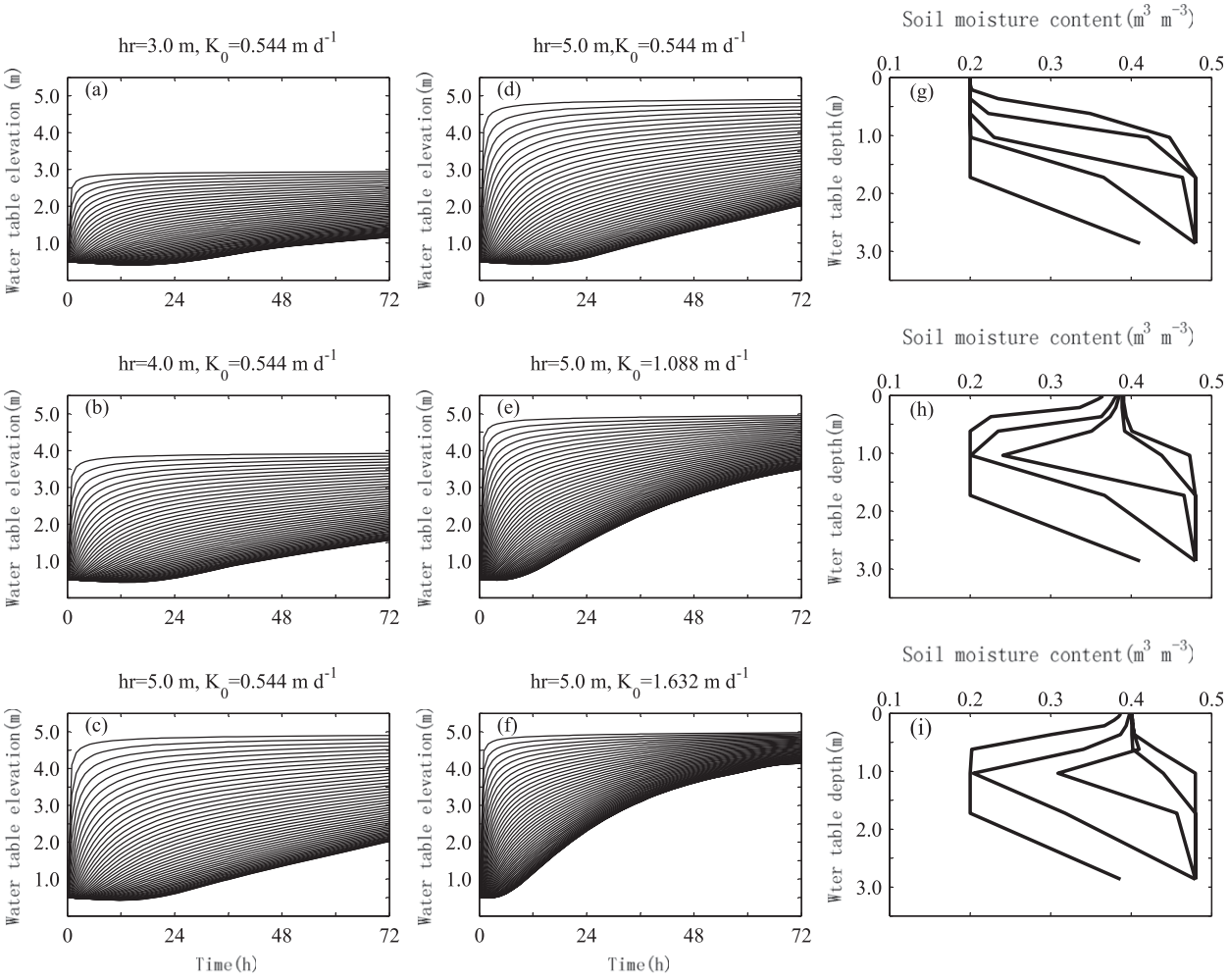

FIG. 6. (a)–(c) The water table elevation curved lines of the soil vertical profile cells in 3 days with different fixed uniform river elevations, and each line denotes the variation in the water table elevation in one cell; (d)–(f) as in (a)–(c) but with different surface hydraulic conductivities (with units of m day^{-1}); and (g)–(i) soil moisture profiles of the soil column 20 m from the river bank every 2 days over 10 days when the surface flux was $P - E - R = 0.0$, 0.1, and 0.15 cm h^{-1}, respectively.

vertical hydraulic conductivity, ψ_s is the saturated water potential, θ_s is the saturated soil moisture content, and b is the soil pore size index. These soil parameter values were adopted as follows: $\theta_s = 0.48$, $\psi_s = -200$ mm, $K_{s1} = 6.3 \times 10^{-3}$ mm s^{-1}, and $b = 6.0$, which is the sixth of the 12 kinds of soil parameters according to the Biosphere–Atmosphere Transfer Scheme (BATS) soil classification for global soil (Dickinson et al. 1986). The specific yield n_e is 0.25. The initial soil moisture content θ_0 is 0.2. The river elevation was taken as the boundary near the river and zero flux was applied on other parts in the boundary of the reference plane. The terrain slope β was taken as 0, and hence from (26), $f = 120$ m. Here, we discuss the sensitivities of three important parameters: river elevation h_r, ground surface horizontal hydraulic conductivity K_0, and surface flux $P - E - R$, where P is the rainfall reaching the ground surface, E is the ground evaporation, and R is the surface runoff.

We first examine the sensitivity of river elevation. Three fixed uniform river elevations are considered: $h_r = 3$, 4, and 5 m. We assume that the ground surface horizontal isotropic hydraulic conductivity K_0 is equal to 0.544 m day^{-1} and that there is zero flux across the ground surface. For cases in which there is uniform river elevation h_r, horizontal isotropic hydraulic conductivity K_0, and the same initial water table, the water table and the soil moisture at different row cells with equal distances from the river bank are equal. Therefore, water table and soil moisture profiles in the soil vertical profile were used to describe their changes in the three-dimensional zone. As shown in Figs. 6a–c, the elevated value of the water table increases as river elevation

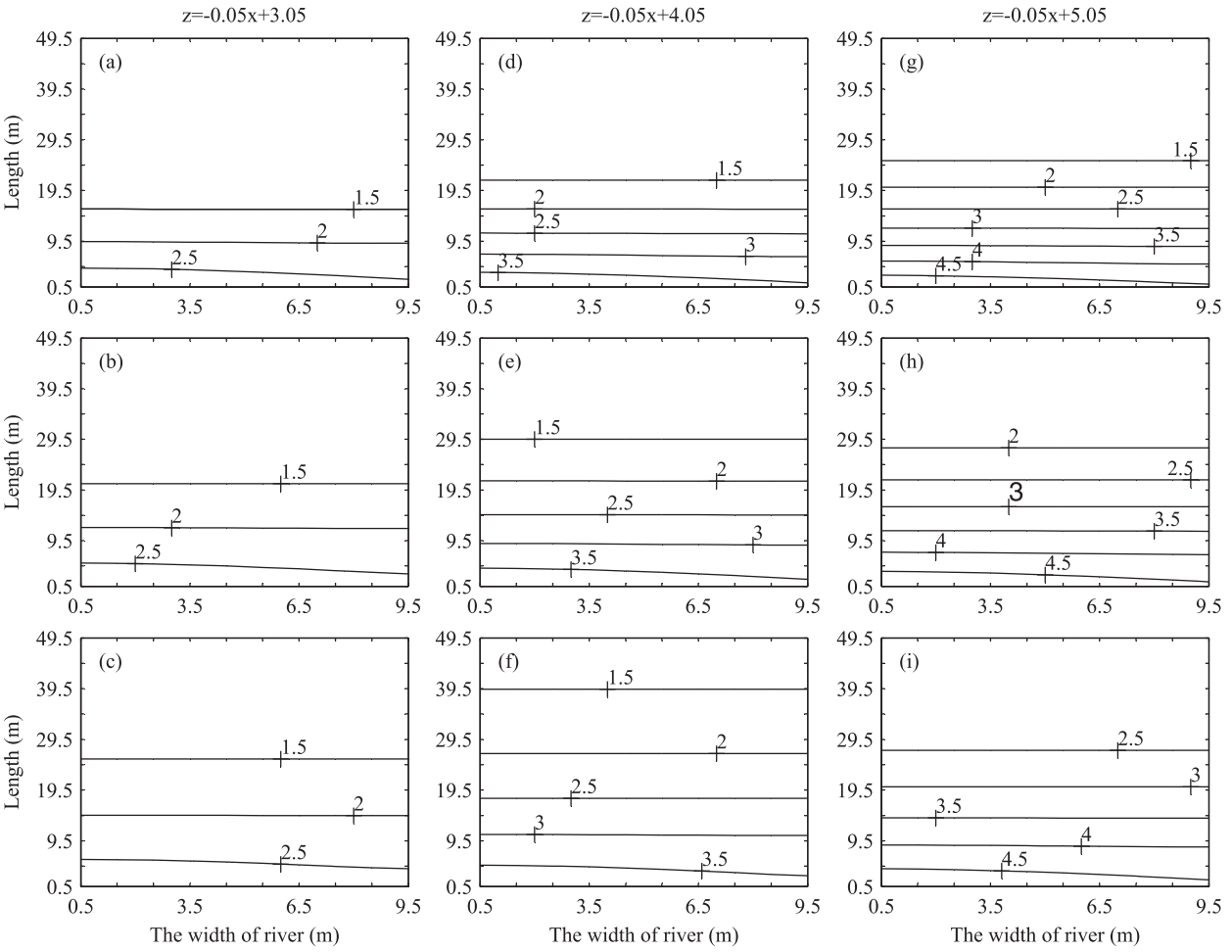

FIG. 7. The water table contour lines for disunity in river elevation over 3 days. (a)–(c) The water table contours for the first, second, and third day, respectively, and the river elevation with $z = -0.05y + 3.05$; (d)–(f) as in (a)–(c) but with $z = -0.05y + 4.05$; and (g)–(i) as in (a)–(c) but with $z = -0.05y + 5.05$.

increases. This is because a high river elevation enhances the hydraulic gradient between the river cell and study cells, making the groundwater flow stronger.

Next, the sensitivity of the ground surface horizontal hydraulic conductivity K_0 was examined. As shown in Eq. (25), the groundwater horizontal hydraulic conductivity K_s at depth z is determined by K_0 for fixed f, so the variation of K_0 can cause changes in K_s, and the lateral flow was also changed. We consider the cases where river elevation $h_r = 5$ m and the ground surface horizontal hydraulic conductivity $K_0 = 0.544$, 1.088, and 1.632 m day^{-1}, with the same initial values and boundary conditions, as well as the same soil parameters values (except K_0) as those in the experiments for the sensitivity of river elevation. The results are shown in Figs. 6d–f, which indicates that the difference in water table elevations for grid cells with different distances from the river decreases as the hydraulic conductivity increases. This is because the increased groundwater hydraulic conductivity reduces the response time of the flow exchange between grid cells.

To examine the sensitivity of the surface flux, the surface infiltration flux is considered: $P - E - R = 0.0$, 0.1, and 0.15 cm h^{-1} with the same soil parameters, initial values, and boundary conditions as described in Fig. 6d. The soil moisture profiles in the soil column 20 m from the river bank every 2 days for 10 days are shown in Figs. 6g–i for different infiltration fluxes. The results showed that both soil moisture content and water table elevations increase as surface infiltration increases. Because water table elevations and soil moisture content are equal in row cells, each curved line in Fig. 6 actually reflects the results of the curved surface in the three-dimensional zone.

We examined the case in which river elevations have a linear relationship with a length along a river and

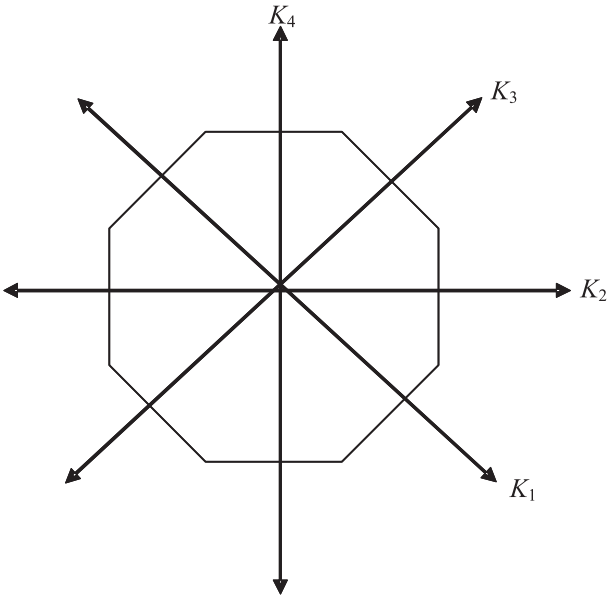

FIG. 8. Hydraulic conductivity across eight sides.

surface hydraulic conductivity K_0 is still isotropic in the horizontal direction. We assumed that the river elevations have a linear relationship given by the following three cases: $z = -0.05y + 3.05$, $z = -0.05y + 4.05$, and $z = -0.05y + 5.05$. Other soil parameter values, initial values, and boundary conditions were the same as those described in Fig. 6d. The contour lines of the water table elevations for different river relationships are shown in Fig. 7. From the three subplots on the left, we can see that water table elevations increase as time increases. This conclusion is also suitable for river relationships $z = -0.05y + 4.05$ and $z = -0.05y + 5.05$, the results of which are shown in the middle and on the right of Fig. 7, respectively. As shown in the rows, if the river elevations are higher, the water table elevations have a greater increase. Because of disunity in river elevations, the contour line near the river bank is bent. This is because high river elevation cells provide more recharge to the aquifer cells. Because the water table in each cell is determined by the eight neighbor cells, the effect of different river elevations on aquifer cells is weakened as flow distance increases, and thus the contour lines far from the river are nearly straight.

Finally, the ground surface anisotropic hydraulic conductivity in the horizontal direction was examined. As shown in Fig. 8, there are four different hydraulic conductivities through eight edges in a cell, assuming the value of the hydraulic conductivity equals that in the opposite direction. Hydraulic conductivities K_2 and K_4 parallel the x axis and y axis, respectively, and K_1 and K_3 are at a 45° angle to the x axis in the clockwise and counterclockwise directions, respectively. Although K_i ($i = 1, 2, 3, 4$) in a cell is different, they are correspondingly equal in row cells. Other soil parameter values, initial water table elevations and soil moisture content, and boundary conditions are also the same as described in Fig. 6d, except for hydraulic conductivity. River elevations are assumed to be uniform 5 m and zero flux is adopted on other parts of the boundary; therefore, the water table elevations in each row are still equal for different K_i ($i = 1, 2, 3, 4$), and the water table elevation lines in the x–z profile can be used to analyze the sensitivity of anisotropic hydraulic conductivity. Four group experiments are shown in Table 1. In the first group of experiments, we consider K_i ($I = 2, 3, 4$) = 0.5 m day^{-1}, and that K_1 is 0.5, 1.0, and 1.5 m day^{-1}. Figures 9a–c shows the water table elevation lines on 3 days for different K_1 values. The water table elevations increase as K_1 increases. As shown in Figs. 9a–c, the water table elevations for the dashed line (i.e., K_1 = 0.5 m day^{-1}) rise as time increases. The same is true for the solid line and dotted line corresponding to $K_1 = 1.0$ and 1.5 m day^{-1}, respectively.

TABLE 1. Experiments (Exp) for analyzing the sensitivities of hydraulic conductivities in four directions to the water table elevation.

Name / Hydraulic conductivity (m day^{-1})	Exp 1	Exp 2	Exp 3	Exp 4
K_1	0.5, 1.0, 1.5	0.5	0.5	0.5
K_2	0.5	0.5, 1.0, 1.5	0.5	0.5
K_3	0.5	0.5	0.5, 1.0, 1.5	0.5
K_4	0.5	0.5	0.5	0.5, 1.0, 1.5

In the second group of experiments, we consider K_i ($i = 1, 3, 4$) = 0.5 m day^{-1}, and that K_2 is 0.5, 1.0, and 1.5 m day^{-1}. Figures 9d–f show the water table lines on 3 days for different K_2 values. The water table elevations increase as K_2 increases. As shown in Figs. 9d–f, the water table elevations for the dashed line (i.e., K_2 = 0.5 m day^{-1}) rise in 3 days, which is also true for the solid line and dotted line. A comparison of Figs. 9a–c with Figs. 9d–f reveals that the contribution of K_2 to the increase in the water table elevation is greater than the contribution of K_1. This is because the distance between the river cell node and study cell node in the K_2 direction is shorter than that in the K_1 direction. The flow q is inversely proportional to the distance l according to $q = K(h_r - h)/l$, where h_r is the river elevation. When the increase of K_1 is as that for K_2, the resulting increase of the groundwater lateral flow for K_1 is smaller than that for K_2. If K_1 and K_2 are

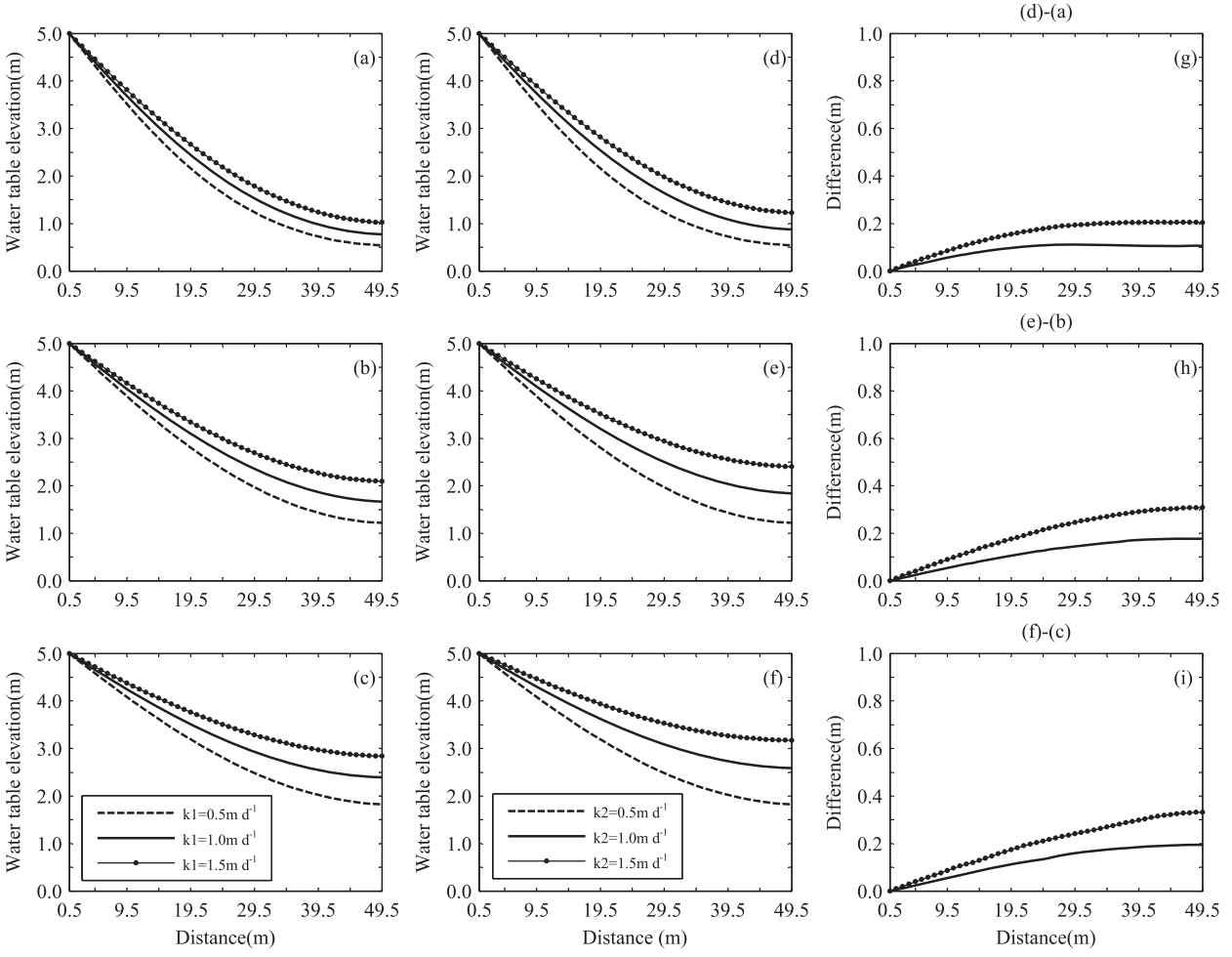

FIG. 9. (a)–(c) The water table elevation profile curved lines with different K_1 for the first, second, and third day, respectively; (d)–(f) as in (a)–(c) but with different K_2; and (g)–(i) the difference in water table elevations between (d)–(f) and (a)–(c).

0.5 m day^{-1}, there is no difference from the case of isotropic hydraulic conductivity.

In the third group of experiments, we consider K_i (i = 1, 2, 4) = 0.5 m day^{-1}, and that K_3 is 0.5, 1.0, and 1.5 m day^{-1}. According to the symmetry, the conclusions are the same as those in the first group of experiments.

In the fourth group of experiments, we consider K_i (i = 1, 2, 3) = 0.5 m day^{-1}, and that K_4 is 0.5, 1.0, and 1.5 m day^{-1}. As the two boundary fluxes paralleling the y axis are zero, the flow between the inner cells in the y direction is zero, and the variation of the water table in row cells is not influenced when K_4 increases. Therefore, the water table elevation lines for K_4 = 0.5, 1.0, and 1.5 m day^{-1}, respectively, and are overlapped at any moment. Figures 9g–i show the differences in water table elevations between Figs. 9d–f and Figs. 9a–c. Because the water table elevations for the two cases of K_1 = 0.5 m day^{-1} and K_3 =0.5 m day^{-1} are equal, the differences between them are zero (no lines are given).

b. *Comparison of the simulations by the quasi-three-dimensional model and a full three-dimensional scheme*

To test feasibility and efficiency of the quasi-three-dimensional model, a numerical experiment by a full three-dimensional scheme was conducted, and the simulation was compared to that by the quasi-three-dimensional model mentioned above. The three-dimensional scheme was derived from the theoretical model of the interaction between soil water and groundwater introduced in section 2, which consists of the three-dimensional Richard's equation (1), the two-dimensional groundwater equation (8), and their vertical exchange flux across the water table in each grid cell. The vertical flux can be obtained by integrating three-dimensional Richard's equation (1)

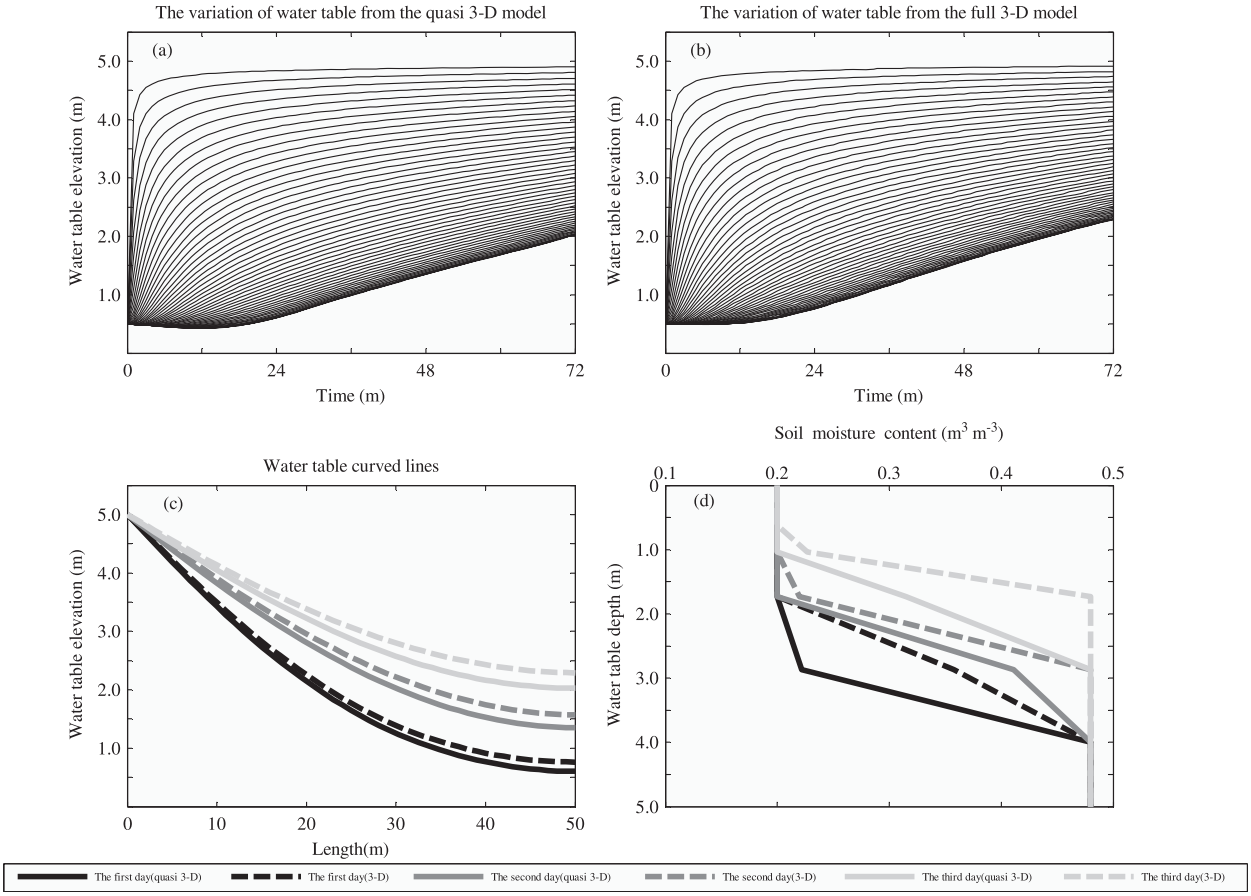

FIG. 10. The comparison of simulation results between the quasi-three-dimensional model and the full three-dimensional model under identical initial and boundary conditions. (a),(b) The simulated water table elevation curved lines of the soil vertical profile at cells in 3 days for the quasi-three-dimensional model and the full three-dimensional scheme, respectively, and each line denotes the variation in the water table elevation in one cell; (c) the comparison of water table curved lines of the soil vertical profile every day over 3 days; and (d) the comparison of soil moisture profiles of the soil column 20 m from the river bank every day over 3 days.

over the unsaturated soil column elevation $[h(x, y, t), H(x, y)]$ as follows:

$$q_{z=h(x,y,t)}(x,y,t) = \int_{h(x,y,t)}^{H(x,y)} \frac{\partial\theta}{\partial t}\,dz - \int_{h(x,y,t)}^{H(x,y)} \frac{\partial}{\partial x}\left[D(\theta)\frac{\partial\theta}{\partial x}\right]dz - \int_{h(x,y,t)}^{H(x,y)} \frac{\partial}{\partial y}\left[D(\theta)\frac{\partial\theta}{\partial y}\right]dz + q_{z=H(x,y)}(x,y,z,t). \quad (27)$$

We chose the study domain to be the same as that of the synthetic experiments mentioned in section 3a (Fig. 5) and all soil parameters, initial values, and boundary conditions the same as those related to Fig. 6d, and then conducted the numerical experiment by the full three-dimensional scheme. From the discussion in the previous subsection, we know that the water table and the soil moisture in different row cells with equal distances from the river bank at any time are equal for a given uniform river elevation and a hydraulic conductivity, the same initial water table, and zero boundary conditions. Therefore, water table elevation and soil moisture content in soil profile can describe their changes in the three-dimensional zone.

The simulated water table elevation and soil moisture by the quasi-three-dimensional model and the full three-dimensional model are shown in Fig. 10. From Figs. 10a–c, we can see that the simulated water table curves by the quasi-three-dimensional scheme have the same character as those by the full three-dimensional model, and the simulated water tables by the full three-dimensional scheme are slightly higher than those by the developed model. This is because latent flows between the unsaturated soil columns by the full three-dimensional scheme increase the supply of soil water to water table under the invariable river elevation. The soil moisture profiles in the soil column at 20 m from the river bank

are shown in Fig. 10d, which indicates that the simulated soil moisture by the full three-dimensional scheme is higher than that by the quasi-three-dimensional model. Obviously, the increased soil water for unsaturated soil columns comes from the latent flow from the river.

The simulated averagely soil moisture content and water table elevation for 3 days by the full three-dimensional model increase by 3.36×10^{-3} and 0.174 m, respectively, compared to those by the quasi-three-dimensional model. We also find that the central processing unit (CPU) time consumed by the full three-dimensional model is much greater than that by the quasi-three-dimensional model, which shows the feasibility and efficiency of the quasi-three-dimensional model.

c. Model validation

In this subsection, the quasi-three-dimensional model is validated based on an actual case of stream water conveyance in the lower reaches of the Tarim River. The Tarim River basin is one of the most severely ecologically degraded regions in China. Because of climatic factors and unreasonable utilization of the water resource by humans in the upper and middle reaches, the river dries up and the water table is continuously decreasing because of the lack of supply from the river. As a result, the survival of many plant and animal species in the lower reaches of the Tarim River are threatened (e.g., Song et al. 2000; Feng et al. 2001; Chen et al. 2004). Since May of 2000, a water conveyance project has been implemented in the lower reaches of the Tarim River. This project supplies the water table on both sides of the river, thereby sustaining the ecological balance in the riparian zone. The project lasted for 934 days, which are divided into eight phases, during which time the total discharge was about 21.96×10^9 m^3. There are nine monitoring cross sections and 40 groundwater monitoring wells in the region to collect river flow and water table elevation data (e.g., Chen et al. 2004; Xu et al. 2003).

The Yingsu section, which is the third of nine sections, is located 60 km from the Daxihaizi Reservoir. We obtained detailed data for the section from four monitoring wells—C3, C4, C5, and C6—which were located 150, 300, 500, and 750 m from the river bank, respectively. We took the aquifer adjoining the river as the study domain. The aquifer is 1000 m long and 50 m wide and includes the Yingsu section (i.e., Fig. 11). Because observation data only exist for the Yingsu section, we assumed that the initial river data or initial water table elevations in the row cells were equal to the initial values of those at the Yingsu section and that groundwater hydraulic conductivity is isotropic. Therefore, the water table elevations in the row cells are equal at any moment, and the water table

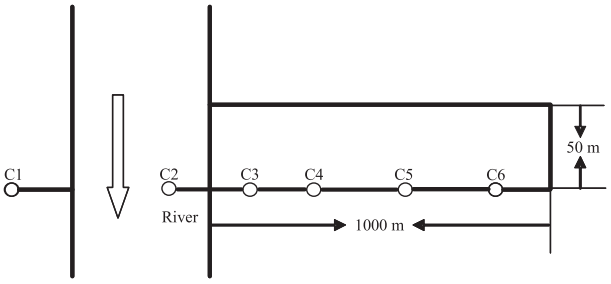

FIG. 11. Schematic representations of the study domain and monitoring wells at Yingsu section.

elevation line in the section reflects the water table elevations in the three-dimensional study domain.

The 81 days of data (i.e., from 16 November 2000 to 4 February 2001) obtained from the four monitor wells in the second phase of the water conveyance project were used to calibrate the surface hydraulic conductivity K_0 by the quasi-three-dimensional model. The observed water table elevations of the four monitoring wells from the third phase to the sixth phase were applied to validate the quasi-three-dimensional model with the calibrated K_0.

The observed river elevations and discharges in the eight phases are shown in Fig. 12. Through regression, the fitted index function can be expressed as

$$H(t) = 832.608 + [Q(t)/5.1425]^{0.5075}, \qquad (28)$$

where $H(t)$ is the river elevation and $Q(t)$ is the river discharge.

According to the elevations of the four monitoring wells, the linear regression function for the ground surface elevation at the section is as follows:

$$z(x) = -0.001x + 836.1952, \qquad (29)$$

where x is the perpendicular distance from the river bank and $z(x)$ is the ground surface elevation. This linear function is extended to the ground surface plane for model simulation.

For the lower reaches of the Tarim River, there are no available soil texture classification data for numerical modeling, although the soil characteristics have been studied (Yang et al. 2007). Therefore, based on the 12 types of global soil classification in BATS and the geography position of the Yingsu section, the sixth type of sandy clay loam can be confirmed as $\theta_s = 0.48$, $\psi_s = -200$ mm, $K_s = 6.3 \times 10^{-3}$ mm s^{-1}, and $b = 6.0$. Let $n_e = 0.25$. The initial soil moisture content is deficient; therefore, we set the initial unsaturated soil moisture content at 0.2 and the sink terms $f_1(x, y, z, t)$ and $f_2(x, y, t)$ at zero. The horizontal space step is 10 m, and the

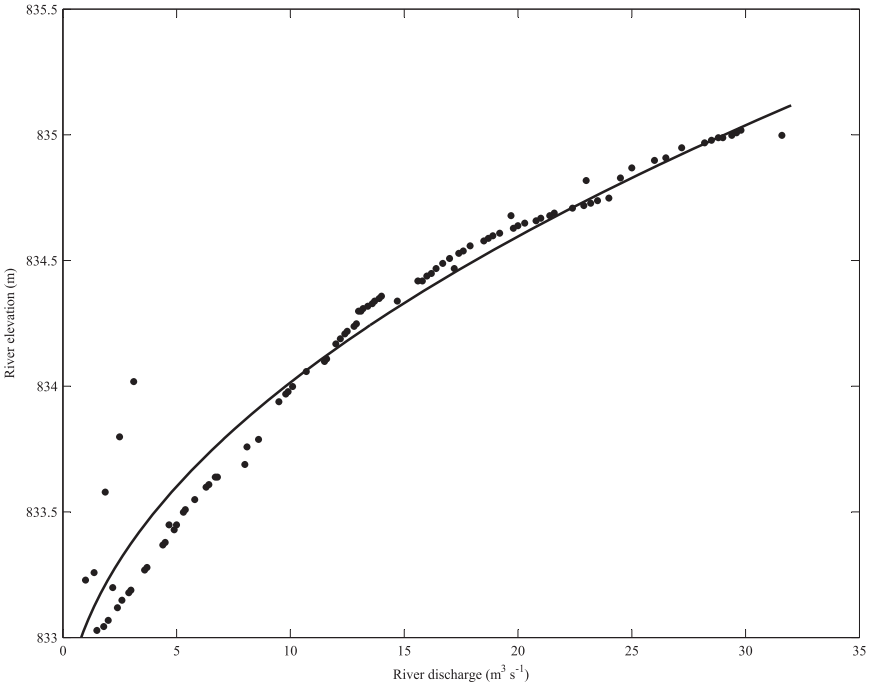

FIG. 12. The relationship between the observed discharges and river elevations (dots), and their fitted rating curve (solid line).

vertical space step adopts the developed structure. Generally, ground evapotranspiration and runoff should be obtained by observation or computation of the land surface model. Because the annual precipitation is less than 50 mm and surface runoff is barely formed in this area, we assumed that the surface flux $P - E - R$ is equal to zero.

In the second phase of the water conveyance for calibration, the first day for integrating the model was 16 November 2000. The linear regression function for the initial water table elevation at the Yingsu section is

$$z(x) = -0.0011x + 828.2477, \tag{30}$$

where x is the perpendicular distance between the river bank and the calculation node and $z(x)$ is the water table elevation. This linear function is also extended to be a plane for model simulation.

With the SCE-UA parameter calibration method, some parameters of the quasi-three-dimensional model were determined for the second phase of the water conveyance. In the first case, the ground surface horizontal hydraulic conductivity K_0 in the study domain was determined to be 5.074 m day^{-1} by calibration for the second phase of the water conveyance. In the second case, by calibration, the saturated hydraulic conductivity K_{s1}, the Clapp and Hornberger parameter b, and the ground surface horizontal hydraulic conductivity K_0 were determined to be 1.0×10^{-2} mm s^{-1}, 2.9, and 2.930 m day^{-1}, respectively. Simulations by the quasi-three-dimensional model with the calibrated parameters were then conducted to estimate the variation of water table elevations for the four wells from the second phase to the sixth phase. We call the simulations related to the first and second cases simulation 1 and simulation 2, respectively.

Figure 13 shows the observed water table elevations (dotted line) and the simulated water table elevations (dashed line for simulation 1, solid line for simulation 2) for four wells (C3–C6) in the Yingsu section during the second phase of the water conveyance from 16 November 2000 to 4 February 2001. The simulations were found to agree with the observations in an acceptable fashion. The mean absolute error (MAE), root mean squared error (RMSE), and correlation coefficient (CC) from simulation 1 by the model with the calibrated parameters for the first case are 0.199 m, 0.235 m, and 0.991, respectively. MAE, RMSE, and CC for simulation 2 for the second case are 0.100 m, 0.120 m, and 0.996, respectively.

The simulated water table elevations from the third to the sixth phase are shown in Fig. 14, from which we can see that the simulation results in the third and six phases are better than in the fourth and fifth phases, the simulation results for well C3 are slightly better than for the others, and that the simulation by the model with three

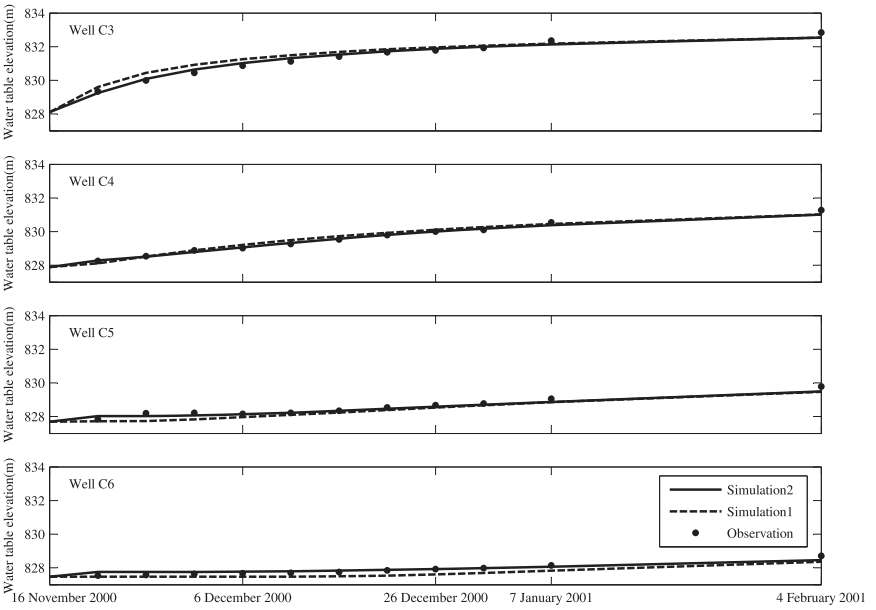

FIG. 13. Time series of the observed and simulated water table elevations for wells C3, C4, C5, and C6 during the second phase of water conveyance.

calibrated parameters for the second case is better than that for the first case except for the sixth phase. The comparison of statistical errors for the six phases is shown in Table 2. Obviously, the multiparameter calibrated model improves the simulation precision to some extent.

d. A numerical experiment for Tarim River basin

In this subsection, a numerical experiment by the model for the Tarim River basin was presented to test the model on simulation of the effects of lateral groundwater flow for large-scale high-relief topography with stream water conveyance. The Tarim River is the principal river of the Xinjiang Uygur Autonomous Region in the People's Republic of China (Fig. 15a). It gives its name to the great Tarim basin between the Tian Shan and Kunlun Mountains systems (the northern edge of the Tibetan Plateau) of Central Asia. It is the longest inland river in China with an annual flow of 4–6 billion cubic meters. The Tarim flows in an eastward direction around the northern edge of the Taklamakan Desert. The total length of the Yarkand–Tarim river system is 2030 km. The area of the Tarim River basin is about 557 000 km^2. The basin is the driest region of Eurasia. The predominant part of it is occupied by the Taklamakan Desert, whose sand area exceeds 270 000 km^2. Precipitation in the Tarim basin is extremely scanty, and in some years it is nonexistent. In the Taklamakan Desert and in the Lop Nur basin, the average annual total of precipitation is about 12 mm. In the foothills and in several other areas of the river's basin, the precipitation amounts to from 50 to 100 mm a year. In the Tian Shan it is much wetter, with precipitation often exceeding 500 mm. The land elevation spans a range from 90 m below sea level to near about 6900 m. We apply the model for the Tarim River basin assuming the vertical exchange flux to be zero at the surface. A grid size of 10 km was selected. The initial water table elevation is assumed to be 20 m below the land surface except that the river elevation is assumed to be 1.0 m below the land surface (i.e., Fig. 15b). The groundwater hydraulic conductivity for the surface soil $K_0 = 10$ m day^{-1} and the e-folding length $f = 120$. The boundary condition for the basin is assumed to be zero flux. Figure 15c shows the water table elevations for 20 years to the initial condition. The differences in water table elevations between Fig. 15c and Fig. 15b are shown in Fig. 15d. It is found that the groundwater flows from high to low altitudes and water tables have an increasing trend around river channels. Because of the initial water table elevation differences between grid cells corresponding to the differences of terrain height, the groundwater in high-altitude areas supply low-altitude areas. At the same time, a stable river elevation supplies water tables near river banks, which results in elevation of water tables near river banks.

4. Conclusions

In this study, a quasi-three-dimensional numerical model for predicting the water table and soil moisture content

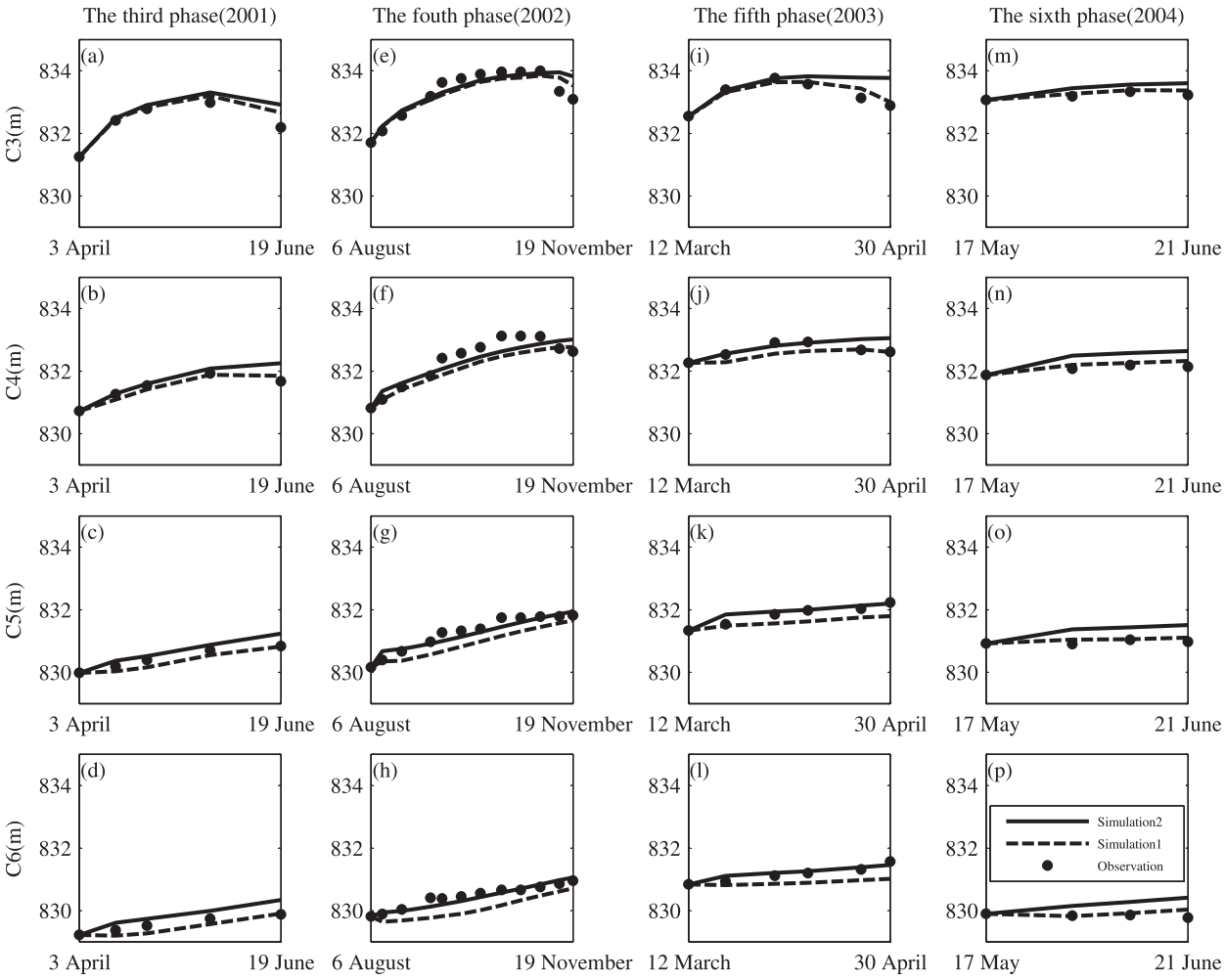

FIG. 14. Observed (dots) and simulated (dashed line and solid line) water table elevations for four monitoring wells from the third phase to the sixth phase. (top)–(bottom) Wells C3, C4, C5, and C6, and (left)–(right) the phases of water conveyance from the third to sixth.

simultaneously is established. Three-dimensional soil water flow in the aquifer zone is divided into one-dimensional vertical soil water flow in unsaturated soil columns and two-dimensional horizontal groundwater flow in the saturated zone. For each unsaturated soil column, a new soil layer structure is presented, and an adaptive grid refinement method is applied to model the soil moisture content at the cell nodes.

Synthetic experiments using the quasi-three-dimensional numerical model were conducted to test the sensitivities

TABLE 2. The comparison of simulation errors between the model with one calibrated parameter and the model with three calibrated parameters for the phase of water conveyance.

Phase	Simulation days	Observation days	MAE	RMSE	CC
2nd	80	12	0.199/0.100	0.235/0.130	0.991/0.996
3rd	77	5	0.123/0.208	0.170/0.289	0.994/0.986
4th	105	12	0.304/0.184	0.360/0.240	0.980/0.981
5th	49	6	0.190/0.160	0.246/0.274	0.980/0.969
6th	35	4	0.080/0.311	0.112/0.372	0.998/0.987

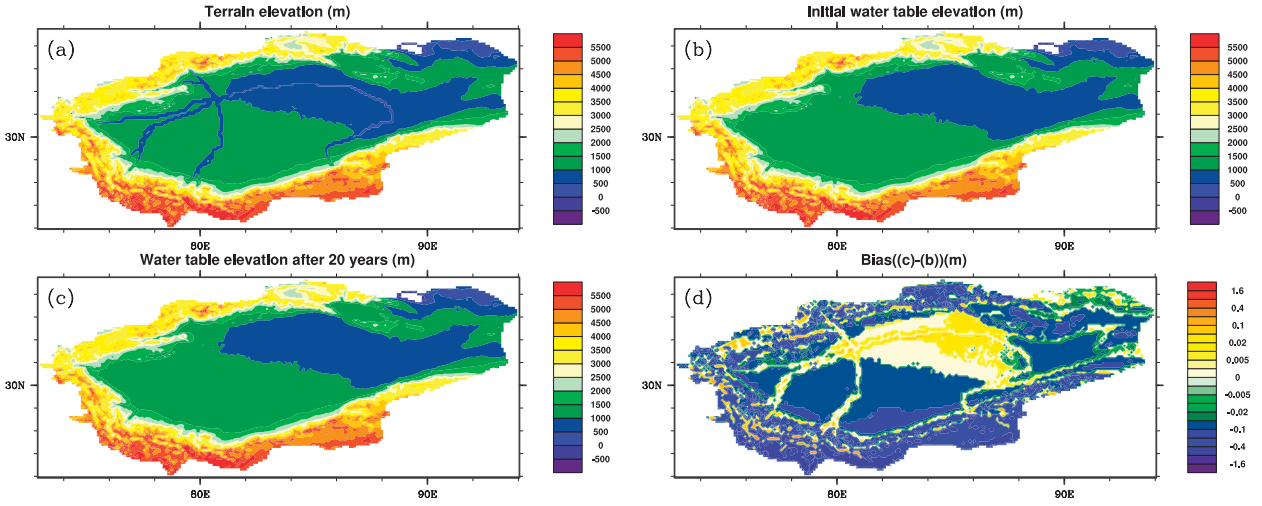

FIG. 15. Water table elevation for Tarim River basin: (a) elevation for Tarim River basin, where color denotes land surface elevation (m), and river channels are highlighted by decreasing 500 m from the land surface; (b) the initial water table elevation (m); (c) water table elevation simulated by model after 20 years to the initial condition; and (d) the bias of water table elevation between (c) and (b).

of the main parameters of the model, which were the river elevation, ground surface horizontal hydraulic conductivity, and surface flux. The results showed the robustness of the developed model under different conditions. A numerical experiment using a full three-dimensional numerical scheme was conducted, and comparison of the simulation by the scheme and that by the quasi-three-dimensional model with the identical initial and boundary conditions demonstrated the feasibility and efficiency of the quasi-three-dimensional model.

The estimation scheme of soil moisture and water table depth based on the developed quasi-three-dimensional model and SCE-UA parameter calibration method was presented and validated by a case of stream water conveyance in the lower reaches of the Tarim River. The simulation results of the water table elevations are in good agreement with the observations in the four monitoring wells. The parameter test and model application for the prediction of water table elevations at the Yingsu section in the lower reaches of the Tarim River show that it can be more reasonable to use the developed model with an adaptive refinement grid to substitute the original 10-layer unsaturated soil water structure, and that the multiparameter calibration for the developed model can improve the simulation precision to some extent. A numerical experiment by the model for the Tarim River basin was conducted to test the model on simulation of the effects of lateral groundwater flow for large-scale high-relief topography with stream water conveyance. The results showed that the model has the potential to be used in large-scale groundwater latent flow.

Acknowledgments. The authors thank Jing Zou for constructive discussions on figure drawing, the editor in chief, Dr. Ana P. Barros, and the two anonymous reviewers for the comments and suggestions on this paper. This study was supported by the National Basic Research Program under Grants 2010CB951001 and 2010CB428403, and by the National Natural Science Foundation of China under Grants 41075062 and 40821092.

REFERENCES

Bear, J., 1972: *Dynamics of Fluids in Porous Media.* American Elsevier Publishing Company, 764 pp.

Chen, J., and P. Kumar, 2001: Topographic influence on the seasonal and interannual variation of water and energy balance of basins in North America. *J. Climate,* **14,** 1989–2014.

Chen, X., and Q. Hu, 2004: Groundwater influences on soil moisture and surface evaporation. *J. Hydrol.,* **297,** 285–300.

Chen, Y. N., W. C. Cui, and Y. M. Zhang, 2003: Utilization of water resources and ecological protection in the Tarim River Basin (in Chinese). *Acta Geol. Sin.,* **58,** 215–222.

——, X. L. Zhang, X. M. Zhu, W. H. Li, Y. M. Zhang, H. L. Xu, H. F. Zhang, and Y. P. Chen, 2004: Analysis on the ecological benefits of the stream water conveyance to the dried-up river of the lower reaches of Tarim River, China. *Sci. China,* **47D,** 1053–1064.

Christiaens, K., and J. Feyen, 2002: Use of sensitivity and uncertainty measures in distributed hydrological modeling with an application to the MIKE SHE model. *Water Resour. Res.,* **38,** 1169, doi:10.1029/2001WR000478.

Clapp, R. B., and G. M. Hornberger, 1978: Empirical equation for some soil hydraulic properties. *Water Resour. Res.,* **14,** 601–604.

Di, Z. H., Z. H. Xie, X. Yuan, X. J. Tian, Z. D. Luo, and Y. N. Chen, 2011: Prediction of water table depths under soil water-ground

water interaction and stream water conveyance. *Sci. China,* **53D,** 420–430, doi:10.1007/s11430-010-4050-8.

Dickinson, R. E., A. Henderson-Sellers, P. J. Kennedy, and M. F. Wilson, 1986: Biosphere atmosphere transfer scheme (BATS) for NCAR community climate model. NCAR Tech. Note. NCAR/TN-275+STR, 69 pp.

Duan, Q. Y., S. Sorooshian, and V. K. Gupta, 1992: Effective and efficient global optimization for conceptual rainfall-runoff model. *Water Resour. Res.,* **28,** 1015–1031.

——, ——, and ——, 1994: Optimal use of the SCE-UA global optimization method for calibrating watershed models. *J. Hydrol.,* **158,** 265–284.

Fan, Y., G. Miguez-Macho, C. P. Weaver, R. Walko, and A. Robock, 2007: Incorporating water table dynamics in climate modeling: 1. Water table observations and equilibrium water table simulations. *J. Geophys. Res.,* **112,** D10125, doi:10.1029/2006JD008111.

Feng, Q., K. N. Endo, and G. D. Cheng, 2001: Towards sustainable development of the environmentally degraded arid rivers of China—A case study from Tarim River. *Environ. Geol.,* **41,** 229–238.

Ferguson, I. M., and R. M. Maxwell, 2010: Role of groundwater in watershed response and land surface feedbacks under climate change. *Water Resour. Res.,* **46,** W00F02, doi:10.1029/2009WR008616.

Gedney, N., and P. Cox, 2003: The sensitivity of global climate model simulations to the representation of soil moisture heterogeneity. *J. Hydrometeor.,* **4,** 1265–1275.

Ivanov, V. Y., E. R. Vivoni, R. L. Bras, and D. Entekhabi, 2004a: Catchment hydrologic response with a fully distributed triangulated irregular network model. *Water Resour. Res.,* **40,** W11102, doi:10.1029/2004WR003218.

——, ——, ——, and ——, 2004b: Preserving high-resolution surface and rainfall data in operational-scale basin hydrology: A fully-distributed physically-based approach. *J. Hydrol.,* **298,** 80–111.

Jones, J. P., E. A. Sudicky, and R. G. McLaren, 2008: Application of a fully-integrated surface-subsurface flow model at the watershed-scale: A case study. *Water Resour. Res.,* **44,** W03407, doi:10.1029/2006WR005603.

Kollet, S. J., and R. M. Maxwell, 2006: Integrated surface–groundwater flow modeling: A free-surface overland flow boundary condition in a parallel groundwater flow model. *Adv. Water Resour.,* **29,** 945–958.

——, and ——, 2008: Capturing the influence of groundwater dynamics on land surface processes using an integrated, distributed watershed model. *Water Resour. Res.,* **44,** W02402, doi:10.1029/2007WR006004.

Koster, R. D., M. J. Suarez, A. Ducharne, M. Stieglitz, and P. Kumar, 2000: A catchment-based approach to modeling land surface processes in a general circulation model. 1. Model structure. *J. Geophys. Res.,* **105,** 24 809–24 822.

Lei, Z. D., S. X. Yang, and S. Z. Xie, 1987: The equations for unsaturated soil water dynamics (in Chinese). *Dynamics of Unsaturated Soil Water,* S. X. Yang, Ed., Tsinghua University Press, 34–42.

Levine, J. B., and G. D. Salvucci, 1999: Equilibrium analysis of groundwater–vadose zone interactions and the resulting spatial distribution of hydrologic fluxes across a Canadian prairie. *Water Resour. Res.,* **35,** 1369–1383.

Liang, X., and Z. H. Xie, 2003: Important factors in land–atmosphere interactions: Surface runoff generations and interactions between surface and groundwater. *Global Planet. Change,* **38,** 101–114.

——, ——, and Y. M. Huang, 2003: A new parameterization for surface and groundwater interactions and its impact on water budgets with the variable infiltration capacity (VIC) land surface model. *J. Geophys. Res.,* **108,** 8613–8629.

Maxwell, R., and N. Miller, 2005: Development of a coupled land surface and groundwater model. *J. Hydrometeor.,* **6,** 233–247.

——, F. K. Chow, and S. J. Kollet, 2007: The groundwater–land-surface–atmosphere connection: Soil moisture effects on the atmospheric boundary layer in fully-coupled simulations. *Adv. Water Resour.,* **30,** 2447–2466.

Miguez-Macho, G., Y. Fan, C. P. Weaver, R. Walko, and A. Robock, 2007: Incorporating water table dynamics in climate modeling: 2. Formulation, validation, and soil moisture simulation. *J. Geophys. Res.,* **112,** D13108, doi:10.1029/2006JD008112.

Niu, G.-Y., Z.-L. Yang, R. E. Dickinson, L. E. Gulden, and H. Su, 2007: Development of a simple groundwater model for use in climate models and evaluation with Gravity Recovery and Climate Experiment data. *J. Geophys. Res.,* **112,** D07103, doi:10.1029/2006JD007522.

Oleson, K. W., and Coauthors, 2004: Technical description of the Community Land Model (CLM). NCAR Tech. Note NCAR/TN-461+STR, 82 pp.

Qu, Y., and C. J. Duffy, 2007: A semidiscrete finite volume formulation for multiprocess watershed simulation. *Water Resour. Res.,* **43,** W08419, doi:10.1029/2006WR005752.

Rigon, R., G. Bertoldi, and T. M. Over, 2006: GEOtop: A distributed hydrological model with coupled water and energy budgets. *J. Hydrometeor.,* **7,** 371–388.

Salvucci, G. D., and D. Entekhabi, 1995: Hillslope and climatic controls on hydrologic fluxes. *Water Resour. Res.,* **31,** 1725–1739.

Seuffert, G., P. Gross, C. Simmer, and E. Wood, 2002: The influence of hydrologic modeling on the predicted local weather: Two-way coupling of a mesoscale weather prediction model and a land surface hydrologic model. *J. Hydrometeor.,* **3,** 505–523.

Shen, Z. L., G. Y. Liu, C. T. Yang, S. X. Sun, and B. R. Chen, 1982: Groundwater flow movement equation (in Chinese). *Hydrogeology,* Z. L. Shen, Ed., Science Press, 249–251.

Song, Y. D., Z. L. Fan, and Z. D. Lei, 2000: Sustainable development of water resource, socio-economic and ecological environment in Tarim River Basin (in Chinese). *The Water Resource and Ecology in Tarim River,* D. G. Yang et al., Eds., Xinjiang People Press, 310–332.

Sophocleous, M., 2002: Interactions between groundwater and surface water: The state of the science. *Hydrogeol. J.,* **10,** 52–67.

Tian, X. J., Z. H. Xie, S. L. Zhang, and M. L. Liang, 2006: A subsurface runoff parameterization with water storage and recharge based on the Boussinesq-storage equation for a land surface model. *Sci. China,* **49D,** 622–631.

Vivoni, E. R., D. Entekhabi, R. L. Bras, and V. Y. Ivanov, 2007: Controls on runoff generation and scale-dependence in a distributed hydrologic model. *Hydrol. Earth Syst. Sci.,* **4,** 983–1029.

Walko, R. L., and Coauthors, 2000: Coupled atmosphere–biophysics–hydrology models for environmental modeling. *J. Appl. Meteor.,* **39,** 931–944.

Xie, Z. H., and X. Yuan, 2010: Prediction of water table under stream–aquifer interactions over an arid region. *Hydrol. Processes,* **24,** 160–169.

——, Q. C. Zeng, and Y. J. Dai, 1998: Numerical simulation of an unsaturated flow equation. *Sci. China,* **41D,** 429–436.

Xu, H. L., Y. N. Chen, and W. H. Li, 2003: Study on response of groundwater after ecological water transport in the lower reaches of the Tarim River (in Chinese). *Res. J. Environ. Sci.,* **16,** 19–28.

Xue, Y. Q., X. Y. Zhu, J. C. Wu, T. B. Li, S. Z. Lin, and G. T. Jia, 1997: Several problem of groundwater movement (in Chinese). *Groundwater Dynamics,* X. Y. Zhu, Ed., Geological Publishing House, 165–167.

Yang, H. W., and Z. H. Xie, 2003: A new method to dynamically simulate groundwater table in land surface model VIC. *Prog. Nat. Sci.,* **13,** 819–825.

Yang, Y. H., Y. N. Chen, and W. H. Li, 2007: Soil properties and degree of desertification in lower reaches of Tarim River (in Chinese). *J. Soil Water Conserv.,* **21,** 44–49.

Yang, Z.-L., and G.-Y. Niu, 2003: The Versatile Integrator of Surface and Atmosphere processes: Part 1. Model description. *Global Planet. Change,* **38,** 175–189.

Yeh, P., and E. Eltahir, 2005a: Representation of water table dynamics in a land surface scheme. Part I: Model development. *J. Climate,* **18,** 1861–1880.

——, and ——, 2005b: Representation of water table dynamics in a land surface scheme. Part II: Subgrid variability. *J. Climate,* **18,** 1881–1901.

York, J. P., M. Person, W. J. Gutowski, and T. C. Winter, 2002: Putting aquifers into atmospheric simulation models: An example from the Mill Creek Watershed, northeastern Kansas. *Adv. Water Resour.,* **25,** 221–238.

Yuan, X., Z. H. Xie, and M. L. Liang, 2008a: Spatiotemporal prediction of shallow water table depths in continental China. *Water Resour. Res.,* **44,** W04414, doi:10.1029/2006WR005453.

——, ——, J. Zheng, X. J. Tian, and Z. L. Yang, 2008b: Effects of water table dynamics on regional climate: A case study over east Asian monsoon area. *J. Geophys. Res.,* **113,** D21112, doi:10.1029/2008JD010180.